long-wavelength part of the spectrum, and hence was attributed to variation of the depletion-layer width with carrier concentration.

Under irradiation from a xenon arc source, rutile wafers fluorinated at 575 °C produced almost twice the photocurrent obtained from rutile reduced at the optimum temperature (600 °C). The long-wavelength photoresponse was significantly enhanced in the fluorinated material, presumably by the filling of the oxygen vacancies. This enhancement would become appreciably more pronounced under solar irradiation, which provides considerably less relative power at wavelengths below 350 nm.

The long-term stability of fluorinated electrodes in a suitable electrolyte under conditions of intense irradiation and extreme anodic bias was found to be at least as good as that of an optimally reduced electrode. Hydrolysis of the electrodes was completely suppressed by maintaining an adequate concentration of fluoride ions in the aqueous electrolyte. Furthermore, it should be noted that the fluorinated material produced a higher photocurrent than the reduced electrode even after 4 h of operation in the sodium acetate solution. Thus it appears that definite improvement over the photoelectric efficiency of reduced rutile electrodes can be achieved by fluorination.

Acknowledgment. The office of Naval Research, Arlington, Va., supported the work of S.N.S. and K.D. Acknowledgment is made to the National Science Foundation for the support of Y.H.Y. In addition, the authors would like to acknowledge the support of the Materials Research Laboratory Program at Brown University. The authors also wish to express their support to Dr. W. Godek for his assistance with the development of a method for fluorine analysis.

Registry No. TiO_2, 13463-67-7; fluorine, 7782-41-4.

References and Notes

(1) L. A. Harris and R. H. Wilson, *J. Electrochem. Soc.*, **123**, 1010 (1976); L. A. Harris, D. R. Cross, and M. E. Gerstner, *ibid.*, **124**, 839 (1977).
(2) C. E. Derrington, W. S. Godek, C. A. Castro, and A. Wold, *Inorg. Chem.*, **17**, 977 (1978).
(3) L. J. Van der Pauw, *Phillips Tech. Rev.*, **20**, 220 (1958).
(4) G. A. Acket and J. Volger, *Phys. Lett.*, **8**, 244 (1964); V. N. Bogomolov and V. P. Zhuze, *Sov. Phys.—Solid State (Engl. Transl.)*, **8**, 1904 (1967).
(5) S. N. Subbarao, Y. H. Yun, R. Kershaw, K. Dwight, and A. Wold, to be submitted for publication.
(6) J. F. Dewald, *J. Phys. Chem. Solids*, **14**, 155 (1960).

Contribution from the Departments of Chemistry, Howard University, Washington, D.C., and University of Virginia, Charlottesville, Virginia 22901

Magnetic Properties of Some Monomeric and Dimeric Nickel(II) Complexes $NiLX_2$ (L = 2,9-Dimethyl-1,10-phenanthroline (dmp), 2,2′-Biquinolyl, Bathocuproine; X = Cl, Br, I) and the Crystal Structure of $Ni(dmp)I_2$

RAY J. BUTCHER, CHARLES J. O'CONNOR, and EKK SINN*

Received August 31, 1978

The magnetic properties of a series of nickel(II) complexes with the empirical formula $NiLX_2$ are reported and analyzed in terms of their molecular structures. Here L = 2,9-dimethyl-1,10-phenanthroline (dmp), 2,2′-biquinolyl (biq), or 2,9-dimethyl-4,7-diphenylphenanthroline (bathocuproine, bc) and X = Cl, Br, or I. Some of the complexes are known to be dimeric, some monomeric, and $Ni(dmp)I_2$ is shown to be monomeric by crystal X-ray diffraction. Two of the dimeric complexes, $[Ni(biq)Cl_2]_2$ and $[Ni(dmp)Cl_2]_2$, show significant intramolecular antiferromagnetic interactions, two less strongly linked dimers, $[Ni(bc)Cl_2]_2$ and $[Ni(dmp)Br_2]_2$, show weaker antiferromagnetism, and one probable dimer, $[Ni(bc)Br_2]_2$, is weakly antiferromagnetic. The pseudotetrahedral monomeric complexes $Ni(biq)Br_2$, $Ni(biq)I_2$, $Ni(dmp)I_2$, and $Ni(bc)I_2$ have magnetic properties which qualitatively resemble the weakly antiferromagnetic dimers and are analyzed in terms of spin–orbit coupling. Crystal data for $Ni(dmp)I_2$: $NiI_2N_2C_{14}H_{12}$, space group $P2_1/n$, a = 8.472 (2) Å, b = 14.248 (3) Å, c = 13.516 (3) Å, β = 102.72 (2)°, V = 1591 Å^3, R = 3.5%, 2632 reflections.

Introduction

Magnetic and chemical interactions between dimeric metal complexes have been an area of long-standing interest.[1] Recently the preparation and crystal structure has been reported[2] for a series of nickel(II) compounds of the empirical formula $NiLX_2$. The compounds previously reported are shown to produce dimeric and single monomeric units depending on the ligand or anion. The ligand L may be biquinoline (biq), dimethylphenanthroline (dmp), or bathocuproine (bc); the anion X may be Cl, Br, or I. Another of the structures is reported here along with a detailed analysis of the magnetic properties of each member of the series.

The compounds are most easily studied when grouped as monomers or dimers. All of the chlorides form the dimeric complexes $[NiLCl_2]_2$ with five-coordinate nickel ions and two bridging chlorines. The iodides form the monomeric complexes $NiLI_2$, with the coordination sphere of the nickel ion having distorted tetrahedral symmetry. The bromides occupy the middle ground with $Ni(biq)Br_2$ being monomeric and $[Ni(dmp)Br_2]_2$ and $[Ni(bc)Br_2]_2$ having the dimeric form.

The magnetic properties of $[Ni(dmp)Cl_2]_2$ have been reported previously.[3] Our results agree qualitatively regarding the antiferromagnetic dimeric interactions; however quantitative differences in the data exist (i.e., position and height of the maximum of the susceptibility).

The compounds are analyzed in terms of dimeric or monomeric magnetic theory as required by the symmetry from the crystallographic data, and the crystal structure of the pseudotetrahedral complex (2,9-dimethyl-1,10-phenanthroline)diiodonickel(II), $Ni(dmp)I_2$, is reported.

Experimental Section

Preparation. Both the dimeric and monomeric compounds were prepared by the same method. The nickel halide was dissolved in triethyl orthoformate, and the ligand was dissolved in benzene. The compounds precipitated on mixing the two solutions; they were then recrystallized from nitrobenzene, and crystals suitable for X-ray analysis were obtained.

Magnetic Susceptibility. The magnetic susceptibility was recorded with a superconducting susceptometer[4] in the 4–100 K temperature region. All compounds were measured as powder samples and at fields ranging from 80 to 400 Oe.

Crystal data for (2,9-dimethyl-1,10-phenanthroline)diiodonickel(II), $Ni(dmp)I_2$: $NiI_2N_2C_{14}H_{12}$, yellow-brown crystal, space group $P2_1/n$, a = 8.472 (1) Å, b = 14.248 (3) Å, c = 13.516 (3) Å, β = 102.72 (2)°, V = 1591 Å^3, μ(Mo Kα) = 51.4 cm^{-1}, ρ_{calcd} = 2.18 g cm^{-3}, ρ_{obsd} = 2.21 g cm^{-3}; crystal dimensions (mm from centroid), (110) 0.16, ($\bar{1}\bar{1}$0) 0.16, (1$\bar{1}$0) 0.16, ($\bar{1}$10) 0.16, (011) 0.19, (0$\bar{1}\bar{1}$) 0.19, (01$\bar{1}$) 0.17, (0$\bar{1}$1) 0.17, (10$\bar{1}$) 0.32, ($\bar{1}$01) 0.32; maximum and minimum transmission coefficients are 0.42 and 0.30, respectively.

0020-1669/79/1318-0492$01.00/0

Table I. Positional and Thermal Parameters and Their Estimated Standard Deviations for $[Ni(DMP)I_2]$[a]

atom	x	y	z	U_{11}	U_{22}	U_{33}	U_{12}	U_{13}	U_{23}
I(1)	0.16641 (6)	0.34654 (3)	0.42783 (3)	0.0647 (3)	0.0520 (2)	0.0531 (2)	0.0034 (2)	0.0007 (2)	0.0002 (2)
I(2)	−0.33004 (5)	0.35260 (3)	0.21596 (3)	0.0454 (2)	0.0460 (2)	0.0632 (2)	−0.0020 (2)	0.0093 (2)	0.0090 (2)
NI	−0.02395 (9)	0.35228 (5)	0.25358 (4)	0.0476 (4)	0.0343 (3)	0.0421 (3)	−0.0006 (3)	0.0191 (3)	0.0010 (3)
N(1)	0.0660 (5)	0.4542 (3)	0.1820 (3)	0.032 (2)	0.031 (2)	0.043 (2)	−0.001 (2)	0.007 (2)	0.004 (2)
N(2)	0.0640 (5)	0.2683 (3)	0.1595 (3)	0.033 (2)	0.033 (2)	0.038 (2)	0.001 (2)	0.007 (2)	0.002 (2)
C(2)	0.0596 (7)	0.5452 (4)	0.1960 (4)	0.044 (3)	0.033 (3)	0.054 (3)	0.000 (3)	0.001 (3)	−0.003 (2)
C(3)	0.1314 (8)	0.6082 (4)	0.1365 (4)	0.050 (3)	0.029 (3)	0.068 (3)	−0.010 (3)	0.004 (3)	0.006 (3)
C(4)	0.2122 (7)	0.5735 (4)	0.0654 (4)	0.042 (3)	0.043 (3)	0.058 (3)	−0.007 (3)	−0.002 (3)	0.013 (3)
C(5)	0.3015 (7)	0.4307 (5)	−0.0192 (3)	0.041 (3)	0.067 (4)	0.046 (3)	−0.007 (3)	0.013 (2)	0.012 (3)
C(6)	0.3014 (8)	0.3386 (4)	−0.0276 (3)	0.054 (3)	0.064 (4)	0.046 (2)	0.007 (3)	0.023 (2)	0.006 (3)
C(7)	0.2132 (8)	0.1789 (4)	0.0221 (3)	0.054 (3)	0.047 (3)	0.046 (3)	0.014 (3)	0.011 (3)	−0.009 (3)
C(8)	0.1323 (8)	0.1305 (4)	0.0797 (4)	0.062 (4)	0.039 (3)	0.054 (3)	0.005 (3)	0.015 (3)	−0.002 (3)
C(9)	0.0543 (7)	0.1751 (4)	0.1487 (4)	0.048 (3)	0.032 (2)	0.043 (2)	0.002 (2)	0.009 (2)	−0.003 (2)
C(10)	0.2228 (7)	0.2779 (4)	0.0306 (3)	0.042 (3)	0.048 (3)	0.037 (2)	0.005 (3)	0.013 (2)	0.002 (2)
C(11)	0.1446 (6)	0.3189 (4)	0.1017 (3)	0.032 (2)	0.038 (2)	0.034 (2)	0.002 (2)	0.004 (2)	0.006 (2)
C(12)	0.1432 (6)	0.4190 (4)	0.1128 (3)	0.029 (2)	0.039 (3)	0.038 (2)	−0.002 (2)	0.005 (2)	−0.002 (2)
C(13)	0.2220 (7)	0.4747 (4)	0.0530 (4)	0.038 (3)	0.045 (3)	0.043 (2)	−0.006 (3)	0.003 (2)	0.013 (2)
C(14)	−0.0313 (8)	0.5813 (4)	0.2731 (4)	0.057 (3)	0.038 (3)	0.070 (3)	0.004 (3)	0.016 (3)	−0.008 (3)
C(15)	−0.0429 (8)	0.1216 (4)	0.2086 (4)	0.059 (3)	0.040 (3)	0.070 (3)	−0.006 (3)	0.026 (3)	0.004 (3)

atom	x	y	z	B, Å^2	atom	x	y	z	B, Å^2
H(3)	0.104 (5)	0.680 (3)	0.152 (3)	1.6 (8)	H(6)	0.352 (7)	0.301 (4)	−0.064 (3)	5.4 (14)
H(4)	0.251 (8)	0.631 (4)	−0.004 (4)	5.6 (15)	H(7)	0.255 (9)	0.141 (4)	−0.016 (4)	6.0 (17)
H(5)	0.342 (7)	0.481 (4)	−0.062 (4)	4.2 (12)	H(8)	0.101 (8)	0.060 (4)	0.072 (4)	6.2 (16)

[a] $\exp[-1/4(B_{11}h^2a^{*2} + B_{22}k^2b^{*2} + B_{33}l^2c^{*2} + 2B_{12}hka^*b^* + 2B_{13}hla^*c^* + 2B_{23}klb^*c)]$.

The Enraf-Nonius program SEARCH was used to obtain 28 accurately centered reflections which were then used in the program INDEX to obtain approximate cell dimensions and an orientation matrix for data collection. Refined cell dimensions and their estimated standard deviations were obtained from least-squares refinement of 28 accurately centered reflections. The mosaicity of the crystal was examined by the ω-scan technique and judged to be satisfactory.

Collection and Reduction of Data. Diffraction data were collected at 292 K on an Enraf-Nonius four-circle CAD-4 diffractometer controlled by a PDP8/M computer by use of Mo Kα radiation from a highly oriented graphite crystal monochromator. The θ–2θ scan technique was used to record the intensities for all nonequivalent reflections for which $1° < 2\theta < 48°$. Scan widths (SW) were calculated from the formula $SW = A + B \tan\theta$, where A is estimated from the mosaicity of the crystal, and B allows for the increase in width of peak due to $K\alpha_1$–$K\alpha_2$ splitting. The values of A and B were 0.60 and 0.35°, respectively. The calculated scan angle is extended at each side by 25% for background determination (BG_1 and BG_2). The net count is then calculated as $NC = TOT - 2(BG_1 + BG_2)$ where TOT is the integrated peak intensity. Reflection data were considered insignificant if intensities registered less than 10 counts above background on a rapid prescan, such reflections being rejected automatically by the computer.

The intensities of four standard reflections, monitored at 100 reflection intervals, showed no greater fluctuations during the data collection than those expected from Poisson statistics. The raw intensity data were corrected for Lorentz–polarization effects (including the polarization effect of the crystal monochromator) and then for absorption. After the intensities of equivalent reflections were averaged, the data were reduced to 2812 independent intensities of which 2632 had $F_o^2 > 3\sigma(F_o^2)$, where $\sigma(F_o^2)$ was estimated from counting statistics.[5] These data were used in the final refinement of the structural parameters.

Determination and Refinement of the Structure. Full-matrix least-squares refinement was based on F, and the function minimized was $\sum w(|F_o| - |F_c|)^2$. The weights w were taken as $[2F_o/\sigma(F_o^2)]^2$, where $|F_o|$ and $|F_c|$ are the observed and calculated structure factor amplitudes. The atomic scattering factors for nonhydrogen atoms were taken from Cromer and Waber[6] and those for hydrogen from Stewart et al.[7] The effects of anomalous dispersion for all nonhydrogen atoms were included in F_c using the values of Cromer and Ibers[8] for $\Delta f'$ and $\Delta f''$. Agreement factors are defined as $R = \sum||F_o| - |F_c||\sum|F_o|$ and $R_w = (\sum w(|F_o| - |F_c|)^2/\sum w|F_o|^2)^{1/2}$.

Anisotropic temperature factors were introduced for all nonhydrogen atoms. Further Fourier difference functions permitted location of the nonmethyl hydrogen atoms, which were included in the refinement for three cycles of least-squares refinement and then held fixed. The models converged with $R = 3.5\%$, $R_w = 5.0\%$. A structure-factor calculation with all observed and unobserved reflections included (no refinement) gave $R = 3.9\%$; on this basis it was decided that careful measurement of reflections rejected automatically during data collection would not significantly improve the results. A final Fourier difference function was featureless. Tables of the observed structure factors are available.[9] The principal programs used are as described previously.[10]

Table II

Bond Lengths for $Ni(dmp)I_2$ (Å)

Ni-I(1)	2.546 (1)	C(4)-C(13)	1.423 (5)
Ni-I(2)	2.530 (1)	C(5)-C(6)	1.316 (6)
Ni-N(1)	1.987 (3)	C(5)-C(13)	1.445 (5)
Ni-N(2)	2.005 (3)	C(6)-C(10)	1.429 (5)
N(1)-C(2)	1.313 (4)	C(7)-C(8)	1.336 (6)
N(1)-C(12)	1.351 (4)	C(8)-C(9)	1.408 (5)
N(2)-C(9)	1.337 (4)	C(9)-C(15)	1.486 (5)
N(2)-C(11)	1.353 (4)	C(10)-C(11)	1.409 (4)
C(2)-C(3)	1.427 (5)	C(11)-C(12)	1.434 (5)
C(2)-C(14)	1.516 (5)	C(12)-C(13)	1.402 (4)
C(3)-C(4)	1.388 (6)		

Intermolecular Contacts (Å)

I(1)···C(9)	3.935 (2)	$1/2 + x, 1/2 - y, 1/2 + z$
I(1)···C(3)	3.985 (2)	$1/2 - x, y - 1/2, 1/2 - z$
N(1)···C(4)	3.664 (5)	$-x, 1 - y, -z$
C(4)···C(12)	3.418 (5)	$-x, 1 - y, -z$

Results and Discussion

Final positional and thermal parameters for $Ni(dmp)I_2$ are given in Table I. Tables II and III contain the bond lengths and angles. The digits in parentheses in the tables are the estimated standard deviations in the least significant figures quoted and were derived from the inverse matrix in the course of least-squares refinement calculations. Figure 1 shows a stereoscopic view of $Ni(dmp)I_2$, while Figure 2 shows the molecular packing in the unit cell.

The complex consists of discrete monomeric molecules, the closest intermolecular contact involving iodines (3.935 (2) Å) being with a ring carbon of an adjacent molecule. The ligand environment of the nickel atom is a distorted tetrahedron. The Ni–I bonds differ in length (2.546 (1) vs. 2.530 (1) Å) but not as much as do the bridging and nonbridging bonds in the dimeric complexes $[Ni(dmp)Cl_2]_2$ (2.378 (1) vs. 2.414 (1) Å) and $[Ni(dmp)Br_2]_2$ (2.468 (1) vs. 2.649 (1) Å).[2] The two Ni–N bonds are shorter than those in the dimeric chloro and bromo complexes, a fact which is attributed to the reduction

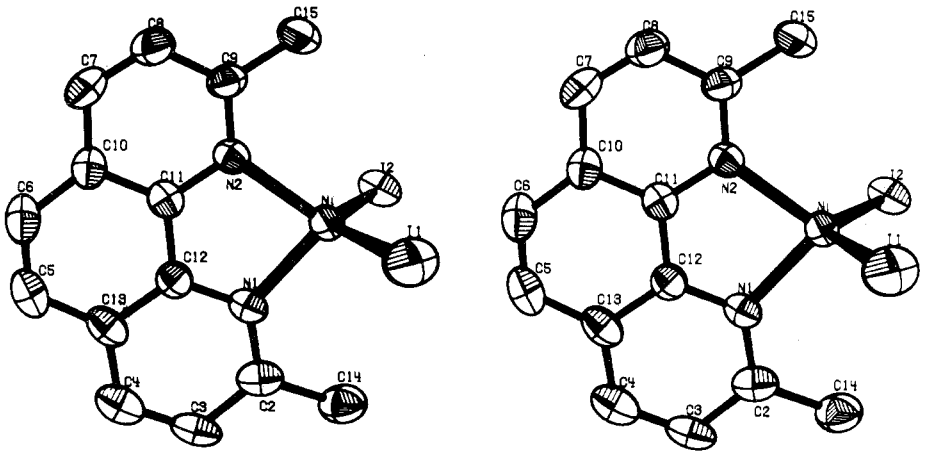

Figure 1. Stereoscopic view of $Ni(dmp)I_2$.

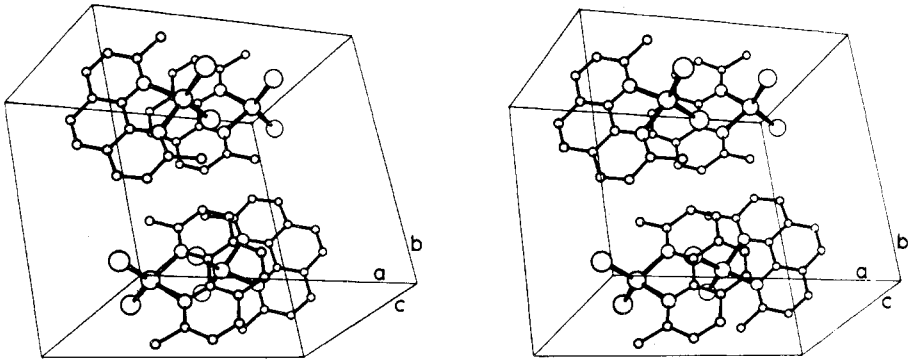

Figure 2. Molecular packing in $Ni(dmp)I_2$.

Table III. Bond Angles (deg) for $Ni(dmp)I_2$

I(1)-Ni-I(2)	126.75 (2)	C(5)-C(6)-C(10)	123.1 (4)
I(1)-Ni-N(1)	103.94 (7)	C(8)-C(7)-C(10)	119.6 (4)
I(1)-Ni-N(2)	108.64 (7)	C(7)-C(8)-C(9)	121.9 (4)
I(2)-Ni-N(1)	112.75 (7)	N(2)-C(9)-C(8)	119.6 (3)
I(2)-Ni-N(2)	112.40 (8)	N(2)-C(9)-C(15)	118.6 (3)
N(1)-Ni-N(2)	83.8 (1)	C(8)-C(9)-C(15)	121.8 (3)
Ni-N(1)-C(2)	128.3 (2)	C(6)-C(10)-C(7)	125.7 (3)
Ni-N(1)-C(12)	111.2 (2)	C(6)-C(10)-C(11)	118.1 (3)
C(2)-N(1)-C(12)	120.5 (3)	C(7)-C(10)-C(11)	116.2 (3)
Ni-N(2)-C(9)	129.7 (2)	N(2)-C(11)-C(10)	123.1 (3)
Ni-N(2)-C(11)	110.7 (2)	N(2)-C(11)-C(12)	116.9 (3)
C(9)-N(2)-C(11)	119.6 (3)	C(10)-C(11)-C(12)	120.0 (3)
N(1)-C(2)-C(3)	120.3 (3)	N(1)-C(12)-C(11)	117.2 (3)
N(1)-C(2)-C(14)	118.5 (3)	N(1)-C(12)-C(13)	123.7 (3)
C(3)-C(2)-C(14)	121.2 (3)	C(11)-C(12)-C(13)	119.1 (3)
C(2)-C(3)-C(4)	120.2 (3)	C(4)-C(13)-C(5)	123.9 (3)
C(3)-C(4)-C(13)	119.0 (3)	C(4)-C(13)-C(12)	116.4 (3)
C(6)-C(5)-C(13)	120.0 (4)	C(5)-C(13)-C(12)	119.7 (3)

of the coordination number from 5 to 4.

The complex $[Ni(biq)Cl_2]_2$ has been shown to be a chlorine-bridged dimer, while the bromo analogue $Ni(biq)Br_2$ is monomeric. This is presumably due to the larger size of the Br atom than of the Cl atom.[2] By contrast, with the sterically related compound dmp, both the chloro and bromo complexes $[Ni(dmp)X_2]_2$ are dimeric, although the bromo complex has a much weaker bridging bond when compared with the nonbridging Ni–X bond than does the chloro complex. For the dmp ligand, the greater size of Br is sufficient to weaken the bridging, while retaining the dimeric structure. The still greater size of the iodine atoms is sufficient to make the present $Ni(dmp)I_2$ complex monomeric. Thus the structures of related complexes can be predicted from steric reasoning and from magnetic properties, although this is not always unambiguous, as will become apparent below. For example, bc and dmp are normally assumed to form identical structures although the crystal structures of $Ni(bc)X_2$ (X = Cl, Br) have not been determined; yet magnetic properties indicate significant differences between dmp and bc.

Table IV. Curie-Weiss Parameters for Each Compound

	g	Θ, K	$\alpha \times 10^6$, emu/mol
$Ni(biq)Cl_2$	2.38	−14.1	
$Ni(biq)Br_2$	2.13	−1.63	830
$Ni(biq)I_2$	2.17	−1.99	760
$Ni(dmp)Cl_2$	2.26	−19.7	
$Ni(dmp)Br_2$	2.18	−2.97	
$Ni(dmp)I_2$	2.30	−3.26	1160
$Ni(bc)Cl_2$	2.41	−1.41	
$Ni(bc)Br_2$	2.40	−2.93	
$Ni(bc)I_2$	2.30	−3.60	1142

The analysis of the magnetic data was begun using the structural data as a guide for theoretical calculations. In addition to the dimeric or monomeric information, the local nickel ion coordination geometry for the dimers and monomers gives quite different electronic states, and therefore different methods of analysis must be employed to explain the magnetic properties.

Preliminary analysis of the data using the Curie–Weiss law was performed on all of the compounds. In some cases, most notable the tetrahedral monomers, a temperature-independent paramagnetism term (α) was required, and in other cases, large deviations from Curie–Weiss behavior at low temperatures restricted the fitting to only the elevated temperature region above the interaction. The standard Curie–Weiss equation was used.

$$\chi(g, \Theta, \alpha) = \frac{Ng^2\mu_B^2}{3k(T - \Theta)}S(S + 1) + \alpha \qquad (1)$$

In all further discussion, the analysis will be divided into the two sets of compounds.

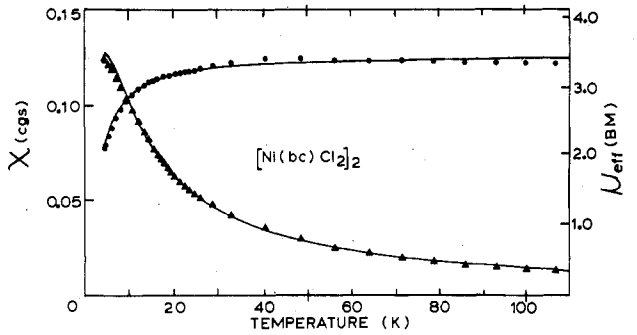

Figure 3. Magnetic susceptibility (▲) and effective magnetic moment (●) plotted as a function of temperature for $[Ni(bc)Cl_2]_2$. The smooth line represents the best fit of the data to $\chi(g, J)$.

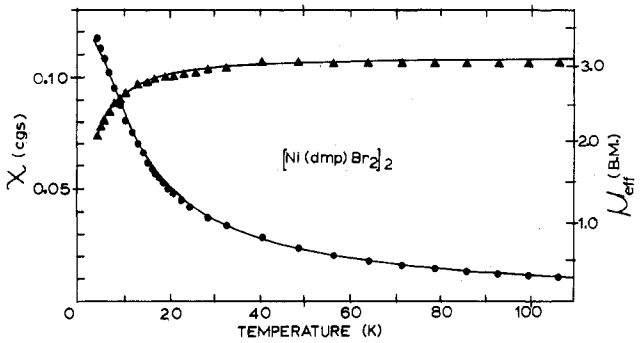

Figure 4. Magnetic susceptibility (●) and effective magnetic moment (▲) plotted as a function of temperature for $[Ni(dmp)Br_2]_2$. The smooth line represents the best fit of the data to $\chi(g, J)$.

Table V. Dimer Magnetic Parameters

	g	J, K	D, K	zJ', K
$Ni(biq)Cl_2$	2.19	−6.97		
	2.31	−7.74	−18.43	0.2
$Ni(dmp)Cl_2$	2.15	−10.0		
	2.21	−10.45	−33.7	1.0
$Ni(bc)Cl_2$	2.45	−2.35		
$Ni(dmp)Br_2$	2.21	−2.18		
$Ni(bc)Br_2$	2.32	−1.12		

The dimeric compounds will be presented first: $[NiLCl_2]_2$ (L = biq, dmp, bc) and $[NiLBr_2]_2$ (L = dmp, bc). For the five-coordinate dimers, the standard dimeric equation for Ni(II) was applied:

$$\chi(g, J) = \frac{Ng^2\mu_B^2}{kT} \frac{5e^{-6J/kT} + e^{-2J/kT}}{5e^{-6J/kT} + 3e^{-2J/kT} + 1} \qquad (2)$$

The pure dimeric interaction was not sufficient to adequately explain the data for the two compounds $[Ni(biq)Cl_2]_2$ and $[Ni(dmp)Cl_2]_2$ which showed a maximum in the experimental susceptibility. For the other dimeric compounds, $[Ni(bc)Cl_2]_2$, $[Ni(dmp)Br_2]_2$, and $[Ni(bc)Br_2]_2$, the characteristic maximum in the susceptibility was not obtained, and the data was adequately fit by the use of only the two parameters of eq 2. These fits are illustrated in Figures 3–5 with plots showing the experimental susceptibility corrected for diamagnetism and the effective magnetic moment as a function of temperature. The calculated values are represented by a smooth line. Better fits could be obtained with the use of more parameters in the equations described below, however the degree of improvement of the fits did not justify the inclusion of these parameters. Indeed, the extra parameters had a tendency to take unrealistic values to increase the closeness of the least-squares fit.

For the two chloride dimers where the maximum is resolved, the situation requires the addition of higher order effects to analyze the data. These compounds have a characteristic shape in the experimental susceptibility vs. temperature curves,

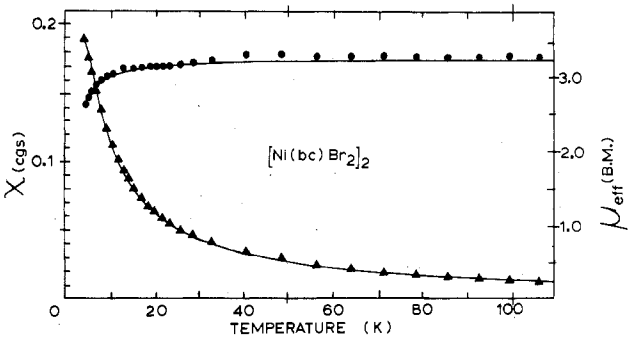

Figure 5. Magnetic susceptibility (▲) and effective magnetic moment (●) plotted as a function of temperature for $[Ni(bc)Br_2]_2$. The smooth line represents the best fit of the data to $\chi(g, J)$.

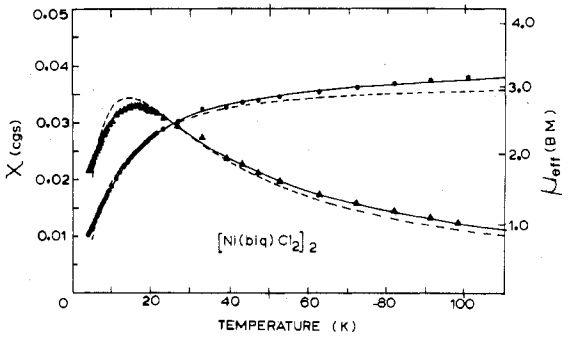

Figure 6. Magnetic susceptibility (▲) and effective magnetic moment (●) plotted as a function of temperature for $[Ni(biq)Cl_2]_2$. The smooth line represents the fit of the data to $\chi(g, J, D, J')$. The dashed line represents the fit of the data to $\chi(g, J)$.

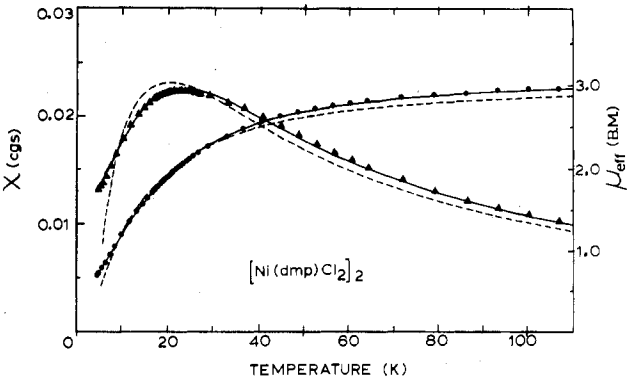

Figure 7. Magnetic susceptibility (▲) and effective magnetic moment (●) plotted as a function of temperature for $[Ni(dmp)Cl_2]_2$. The smooth line represents the fit of the data to $\chi(g, J, D, J')$. The dashed line represents the fit of the data to $\chi(g, J)$.

and the inclusion of additional parameters is justified.

An equation derived by Ginsberg et al.[11] was then applied to the analysis of the data. This equation includes a crystal field splitting term (D) and a molecular field term (zJ'). The equation will be referred to as $\chi(g, J, D, zJ')$. The data for $[Ni(biq)Cl_2]_2$ and $[Ni(dmp)Cl_2]_2$ are plotted in Figures 6 and 7, respectively. The smooth line represents the best fit of the data to the equation of Ginsberg et al. while the dotted line represents the best fit of eq 2 to the data. There is excellent agreement with theory and experiment for $\chi(g, J, D, zJ')$; however the resulting values for D are quite large. The equation was derived from wave functions of axially distorted octahedral symmetry while the coordination sphere of the dimers is five-coordinate, between square planar and trigonal biprism. This would imply the presence of a small amount of spin–orbit coupling and a large rhombic E term which the D term in $\chi(g, J, D, zJ')$ tries to compensate for. The D term then represents a combination of zero-field splitting plus a

spin–orbit coupling contribution, and therefore its magnitude should be judged with caution. The excellent agreement between theoretical values and experimental data indicates that the value of the exchange parameter J obtained from $\chi(g, J, D, zJ')$ should be a good gauge of the exchange between the nickel(II) ions. Attempts were made to analyze the data with other equations that included the dimer interaction plus the molecular field model of interdimer exchange[12] and also a biquadratic exchange term[13] which has nonvanishing matrix elements in a spin $S = 1$ dimer-exchange matrix. These fits were judged to be inferior to those of the Ginsberg equation.

The second class of compounds under study are the monomers composed of $Ni(biq)Br_2$ and $NiLI_2$ (L = biq, dmp, bc). These compounds have a four-coordinate, distorted tetrahedral coordination sphere. Since the symmetry about the nickel ion approaches tetrahedral symmetry, spin–orbit coupling due to a $^3T_1$ ground state should dominate the magnetic properties. In addition to the spin–orbit coupling, a potential field must be added to account for distortions from tetrahedral symmetry. The potential will be approximated as an axial distortion in our calculations.

Calculations on $^3T_1$ ions have been reported previously,[14,15] but for the case with an axial distortion, no simple equation for the susceptibility may be written. The susceptibility must therefore be directly calculated from the eigenvectors and eigenvalues of the electronic Hamiltonian and the $^3T_1$ basis set of wave functions.

The Hamiltonian is then

$$\begin{aligned}\mathcal{H} &= \Delta L_z^2 - \tfrac{1}{3}L^2 + \alpha\lambda L\cdot S \\ &= \Delta L_z^2 - \tfrac{1}{3}L^2 + \alpha\lambda[L_zS_z + \tfrac{1}{2}(L_+S_-) + L_-S_+] \end{aligned} \quad (3)$$

where Δ is the axial crystal-field parameter and λ is the spin–orbit coupling parameter.

The close proximity of $^3T_1$ (^3P) excited states to the $^3T_1$ (^3F) ground state allows significant mixing of the two states. This results in nonintegral eigenvalues when the $^3T_1$ ground-state basis set is operated on by the orbital angular momentum operators in the spin Hamiltonian. Another parameter, α, must be added to account for this effect. α is defined as follows: $L_z|^3T_1\rangle = 0, \pm\alpha|^3T_1\rangle$, where $1.5 > \alpha > 1.0$. Inclusion of the α term in the spin Hamiltonian (3) allows us to use integral orbital eignevalues for the $^3T_1$ ground state. For this type of compound, α typically takes the high-field value of 1.5, and we will use this value in our calculations.

The matrix of $^3T_1$ under the Hamiltonian above can be written in terms of the quantum number M_J (see (A)). The

$$\langle {}^3T_1|\mathcal{H}|{}^3T_1\rangle$$

$$\begin{array}{cccccc} & M_J = 0 & & & M_J = \pm 1 & \quad M_J = \pm 2 \\ |1,-1\rangle & |0,0\rangle & |-1,1\rangle & & |\pm 1,0\rangle \quad |0,\pm 1\rangle & \quad |\pm 1,\pm 1\rangle \\ \begin{bmatrix} \frac{\Delta}{3} - \alpha\lambda & \alpha\lambda & 0 \\ \alpha\lambda & -\frac{2\Delta}{3} & \alpha\lambda \\ 0 & \alpha\lambda & \frac{\Delta}{3} - \alpha\lambda \end{bmatrix} & & & & \begin{bmatrix} \frac{\Delta}{3} & \alpha\lambda \\ \alpha\lambda & -\frac{2\Delta}{3} \end{bmatrix} & \quad \frac{\Delta}{3} + \alpha\lambda \end{array} \quad (A)$$

eigenvalues are given in (B), and the eigenvectors are given

$$\begin{aligned} &\frac{\Delta}{3} + \alpha\lambda \quad \text{twofold degenerate} \\ &{}^1/_2\left[-\frac{\Delta}{3} - \alpha\lambda \pm (\Delta^2 - 2\alpha\lambda + 9\alpha^2\lambda^2)^{1/2}\right] \\ &\frac{\Delta}{3} - \alpha\lambda \\ &{}^1/_2\left[-\frac{\Delta}{3} \pm (\Delta^2 + 4\alpha^2\lambda^2)^{1/2}\right] \text{ each twofold degenerate} \end{aligned} \quad (B)$$

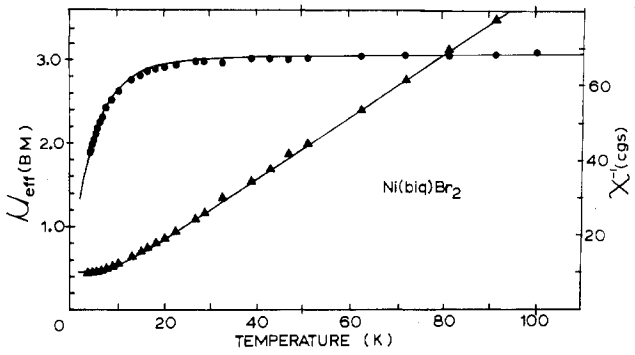

Figure 8. Effective magnetic moment (●) and inverse magnetic susceptibility (▲) plotted as a function of temperature for $Ni(biq)Br_2$. The smooth line represents the fit of the data to eq 4.

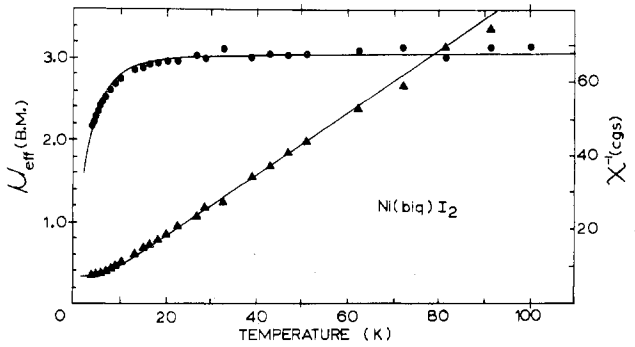

Figure 9. Effective magnetic moment (●) and inverse magnetic susceptibility (▲) plotted as a function of temperature for $Ni(biq)I_2$. The smooth line represents the fit of the data to eq 4.

by a linear combination $\Psi_j = \sum_i c_{ij}\phi_i$ where Ψ_j are the eigenvectors of $^3T_1$ under the Hamiltonian (3) and ϕ_i are the eigenfunctions of the original basis set.

The susceptibility is then calculated by Van Vleck's equation:[16]

$$\chi = \frac{N\sum_j \left[\frac{E_j^{(1)2}}{kT} - 2E_j^{(2)}\right] e^{-E_j^{(0)}/kT}}{\sum_j e^{-E_j^{(0)}/kT}} \quad (4)$$

The energies $E_j^{(0)}$ are the eigenvalues of (B) and $E_j^{(1)}$ and $E_j^{(2)}$ are the first- and second-order Zeeman energies, respectively, and are given by

$$E_j^{(1)} = \langle\Psi_j|\hat{\mu}_i|\Psi_j\rangle \quad (5a)$$

$$E_j^{(2)} = \sum_k \frac{|\langle\Psi_k|\hat{\mu}_i|\Psi_j\rangle|^2}{E_j^{(0)} - E_k^{(0)}} \quad (5b)$$

The moment operator $\hat{\mu}_i$ is given by $\alpha k L_i + 2S_i$ with $i = z$ or x for the parallel and perpendicular axial directions, respectively. In the calculations performed here, it was assumed that the spin–orbit coupling was isotropic ($\lambda_\parallel = \lambda_\perp$).

The susceptibilities were calculated from eq 4 and were fit to the data using a least-squares fitting program. To save computing time, the susceptibility of states with energies greater than $10kT$ were excluded from the summation since they had negligible contribution to the total susceptibility.

The resulting fits are illustrated in Figures 8–11 with the line representing the best fit to eq 4 and the points representing the data. The fitted parameters are shown in Table VI.

Conclusion

The strength of antiferromagnetic interaction is greatly affected by both L and X. For $[NiLCl_2]_2$, where the com-

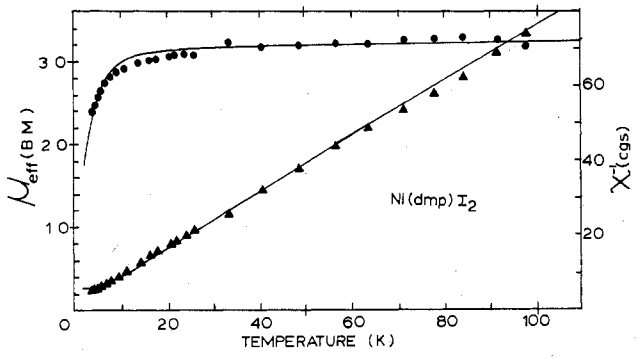

Figure 10. Effective magnetic moment (●) and inverse magnetic susceptibility (▲) plotted as a function of temperature for Ni(dmp)I_2. The smooth line represents the fit of the data to eq 4.

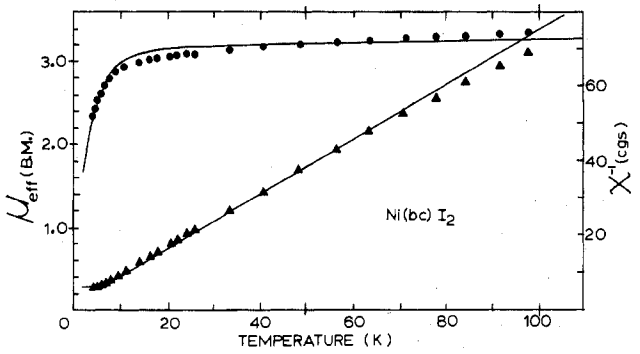

Figure 11. Effective magnetic moment (●) and inverse magnetic susceptibility (▲) plotted as a function of temperature for Ni(bc)I_2. The smooth line represents the fit of the data to eq 4.

Table VI. Spin-Orbit Coupling Parameters for Tetrahedral Monomers

	Δ, K	λ, K	α	*k*
Ni(biq)Br_2	2067	−269	1.0	1.0
		−179	1.5	0.66
Ni(biq)I_2	2789	−247	1.0	1.2
		−165	1.5	0.8
Ni(dmp)I_2	1287	−165	1.0	1.4
		−110	1.5	0.9
Ni(bc)I_2	1267	−172	1.0	1.4
		−115	1.5	0.9

pound is dimeric regardless of L, the ligands may be ordered according to their effect on the magnitude of *J*: dmp > biq > bc. In the cases where the monomer is formed, large distortions from tetrahedral symmetry limit the accuracy of the results, and the fitted parameters should be regarded as an approximate measure of crystal-field strengths.

The series of nine compounds examined here provides a unique medium for the investigation of forces which promote dimer formation. The tendency to split dimeric $NiLX_2$ molecules into two monomers closely parallels the increasing size of the halogen X. For chloro complexes, crystal structures and magnetism in the case of dmp and biq and magnetic properties in the case of bc indicate dimeric structures. For iodo complexes crystal structures (and magnetic properties) indicate monomers for all L. The effect of the ligand L is more subtle: dmp and bc should have identical steric requirements for coordination, and biq should be closely similar, yet the $NiLBr_2$ is monomeric for L = biq and dimeric for L = dmp while for L = bc the magnetism fails to show a dimeric structure unambiguously.

Acknowledgment. Support received under NSF Grant CHE77-01372 is gratefully acknowledged.

Registry No. [Ni(biq)Cl_2]$_2$, 63180-98-3; Ni(biq)Br_2, 14950-13-1; Ni(biq)I_2, 14950-14-2; [Ni(dmp)Cl_2]$_2$, 29115-92-2; [Ni(dmp)Br_2]$_2$, 63180-99-4; Ni(dmp)I_2, 68708-03-2; [Ni(bc)Cl_2]$_2$, 68708-04-3; [Ni(bc)Br_2]$_2$, 68708-05-4; Ni(bc)I_2, 63181-00-0.

Supplementary Material Available: Listings of observed and calculated structure factor amplitudes for Ni(dmp)I_2 (12 pages). Ordering information is given on any current masthead page.

References and Notes

(1) A. P. Ginsberg, *Inorg. Chim. Acta*, **5**, 45 (1971); G. F. Kokoszka and G. Gordon, *Transition Met. Chem.*, **5**, 181 (1969); D. J. Hodgson, *Prog. Inorg. Chem.*, **19**, 173 (1965).
(2) R. J. Butcher and E. Sinn, *Inorg. Chem.*, **16**, 2234 (1977).
(3) E. J. Laskowski, T. R. Felthouse, D. N. Hendrickson, and G. J. Long, *Inorg. Chem.*, **15**, 2908 (1976).
(4) E. J. Cukauskas, B. S. Deaver, Jr., and E. Sinn, *J. Chem. Phys.*, **67**, 1257 (1977).
(5) P. W. R. Corfield, R. J. Doedens, and J. A. Ibers, *Inorg. Chem.*, **6**, 197 (1967).
(6) D. T. Cromer and J. T. Waber, "International Tables for X-ray Crystallography", Vol. 4, Kynoch Press, Birmingham, England, 1974.
(7) R. F. Stewart, E. R. Davidson, and W. T. Simpson, *J. Chem. Phys.*, **42**, 3175 (1965).
(8) D. T. Cromer and J. A. Ibers, ref 6.
(9) Supplementary material.
(10) D. P. Freyberg, G. M. Mockler, and E. Sinn, *J. Chem. Soc., Dalton Trans.*, 447 (1976).
(11) A. P. Ginsberg, R. L. Martin, R. W. Brookes, and R. C. Sherwood, *Inorg. Chem.*, **11**, 2884 (1972).
(12) R. L. Carlin, C. J. O'Connor, and S. N. Bhatia, *J. Am. Chem. Soc.*, **98**, 3523 (1976).
(13) E. A. Harris and J. Owen, *Phys. Rev. Lett.*, **11**, 9 (1963); J. S. Griffith, *Struct. Bonding (Berlin)*, **10**, 87 (1972).
(14) B. N. Figgis, J. Lewis, F. E. Mabbs, and G. A. Webb, *J. Chem. Soc. A*, 1411 (1966).
(15) M. Gerloch and R. C. Slade, *J. Chem. Soc. A*, 1012, 1022 (1969).
(16) J. H. Van Vleck, "The Theory of Electric and Magnetic Susceptibilities", Oxford University Press, London, 1932, p 182.